Received: 14 May 2020 | Revised: 22 June 2020 | Accepted: 11 July 2020

DOI: 10.1002/ardp.202000156

FULL PAPER

DPhG ARCH PHARM
Archiv der Pharmazie

Probing simple structural modification of α-mangostin on its cholinesterase inhibition and cytotoxicity

Kooi-Yeong Khaw[1,2] | Pravin Kumar[3] | Siti Rafidah Yusof[3] | Surash Ramanathan[3] | Vikneswaran Murugaiyah[1]

[1]Discipline of Pharmacology, School of Pharmaceutical Sciences, Penang, Malaysia

[2]School of Pharmacy, Monash University Malaysia, Bandar Sunway, Selangor Darul Ehsan, Malaysia

[3]Centre for Drug Research, Penang, Malaysia

Correspondence
Vikneswaran Murugaiyah, Discipline of Pharmacology, School of Pharmaceutical Sciences, Universiti Sains Malaysia, Penang 11800, Malaysia.
Email: vicky@usm.my

Funding information
Ministry of Higher Education Malaysia and Universiti Sains Malaysia,
Grant/Award Number: No. 1001/PFARMASI/815093

Abstract

α-Mangostin has been reported to possess a broad range of pharmacological effects including potent cholinesterase inhibition, but the development of α-mangostin as a potential lead compound is impeded by its toxicity. The present study investigated the impact of simple structural modification of α-mangostin on its cholinesterase inhibitory activities and toxicity toward neuroblastoma and liver cancer cells. The dialkylated derivatives retained good acetylcholinesterase (AChE) inhibitory activities with IC_{50} values between 4.15 and 6.73 μM, but not butyrylcholinesterase (BChE) inhibitory activities, compared with α-mangostin, a dual inhibitor (IC_{50}: AChE, 2.48 μM; BChE, 5.87 μM). Dialkylation of α-mangostin produced AChE selective inhibitors that formed hydrophobic interactions at the active site of AChE. Interestingly, all four dialkylated derivatives of α-mangostin showed much lower cytotoxicity, being 6.4- to 9.0-fold and 3.8- to 5.5-fold less toxic than their parent compound on neuroblastoma and liver cancer cells, respectively. Likewise, their selectivity index was higher by 1.9- to 4.4-fold; in particular, **A2** and **A4** showed improved selectivity index compared with α-mangostin. Taken together, modification of the hydroxyl groups of α-mangostin at positions C-3 and C-6 greatly influenced its BChE inhibitory and cytotoxic but not its AChE inhibitory activities. These dialkylated derivatives are viable candidates for further structural modification and refinement, worthy in the search of new AChE inhibitors with higher safety margins.

KEYWORDS
acetylcholinesterase, cholinesterase inhibition, cytotoxicity, structural modification, α-mangostin

1 | INTRODUCTION

Xanthones are low-molecular-weight polyphenolic compounds found in plants. They have a nucleus with a dibenzo-α-pyrone scaffold, which is symmetric and occurs as either fully aromatized or as dihydro, tetrahydro, and hexahydro derivatives.[1–5] This family of compounds has numerous pharmacological effects within a notably broad spectrum of diseases, and thus are regarded as privileged structures.[6] Their pharmacological activities are associated with the tricyclic scaffold but vary depending on the nature and/or position of the different substituents.[4,7,8] Naturally occurring xanthone are classified into six groups depending on their chemical framework of the tricyclic scaffold, including the prenylated xanthones, which are restricted to the plant of the family Guttiferae.[9] One of the well-studied prenylated xanthones is α-mangostin, the major xanthone found in *Garcinia mangostana*.

First isolated in 1855, its pharmacological activities have been widely studied in the past two decades. α-Mangostin has 9H-xanthene backbone substituted by a hydroxyl group at positions C-1, C-3, and C-6, a methoxy group at position C-7, an oxo group at position C-9, and

prenyl group at positions C-2 and C-8 (PubChem CID: 5281650). α-Mangostin has been widely reported for its capabilities against several diseases.[10] Among some of its notable effects include anti-inflammatory,[11,12] antioxidant,[13,14] antidiabetic,[15] neuraminidase inhibitory activity,[16] and neuroprotective properties.[17–19] Therefore, further development of α-mangostin as a therapeutic lead compound is of great interest. However, α-mangostin has also been reported to be cytotoxic against a wide range of cell lines such as human breast cancer (MCF-7 and MDA-MB-231), human lung cancer (NCI-H460 and NCI-H187), glioblastoma (SF-268),[20,21] human colon cancer (DLD-1 and HT-29),[22,23] human melanoma (SK-MEL-28), squamous cell carcinoma (A-431),[24] and human leukemia (HL60).[25]

In our continuous search for cholinesterase inhibitors from natural resources, we discovered that α-mangostin is a potent dual cholinesterase inhibitor (IC_{50}: acetylcholinesterase [AChE], 2.14 μM; butyrylcholinesterase [BChE], 5.41 μM).[26] Preliminary structure–activity relationship suggests the importance of the C-8 prenyl and C-7 hydroxyl group for potent AChE and BChE inhibitory activities of the prenylated xanthones from *G. mangostana*. It is reasoned that the cholinesterase inhibitory activities of α-mangostin were lower than that of γ-mangostin due to methoxylation of the hydroxyl group at C-7. Nevertheless, molecular docking revealed that the hydroxyl group of α-mangostin at C-3 and C-6 formed hydrogen bonding within the active site of the AChE and BChE enzymes.[26] However, its cytotoxicity is of great concern and could limit its potential for further development as a cholinesterase inhibitor.

We hypothesized that the pharmacological effects and cytotoxicity of α-mangostin might be attributed at least, in part, by the hydroxyl group at C-3 and C-6 positions. Therefore, in the present study, the impact of simple structural modifications of α-mangostin at C-3 and C-6 on its pharmacological effect and toxicity was investigated. We aimed to semisynthesize α-mangostin derivatives (**A1**–**A4**) via alkylation and evaluated their cholinesterase inhibition versus cytotoxicity. Molecular docking study was carried out to better understand the differences in interactions between enzymes and derivatives. The physicochemical properties of α-mangostin and its derivatives were predicted using Accelrys Discovery Studio software.

2 | RESULTS AND DISCUSSION

2.1 | Chemistry

Semisynthesis of natural compounds is of great interest to a medicinal chemist for one or more of the following reasons: improve bioactivities or simplify the structure while retaining the bioactivity, reduce toxicity, and enhance ADME (absorption, distribution, metabolism, and excretion) properties. A large number of clinically used drugs were semisynthesized natural product analogs. For example, vorapaxar, an antithrombotic agent was semisynthesized from himbacine (a tricyclic lactone from *Galbulimima baccata*).[27] α-Mangostin is a naturally occurring xanthone derived from *G. mangostana*. It possesses favorable pharmacological properties; however, the toxicity feature of this compound may limit its usefulness as a therapeutic drug. Several groups have attempted to semisynthesize α-mangostin derivatives to improve its potency and drug-likeness.[28,29] In the present study, the α-mangostin, obtained from the chloroform fraction of *G. mangostana* fruit pericarp, had undergone simple structural modification of the hydroxyl group at positions C-3 and C-6. The semisynthesized derivatives were obtained via *O*-alkylation reaction with corresponding alkyl halides (methyl-butyl) in acetone under reflux (Scheme 1). The structural characterization of the compounds was determined by nuclear magnetic resonance (NMR) spectroscopy and mass spectrometry.

2.1.1 | Crystal structure of A1

Compound **A1** crystallizes in the triclinic space group P_{-1}. The molecular view of **A1** is shown in Figure 1. The 9H-xanthene ring system is essentially planar, the root mean square deviations being 0.046 Å

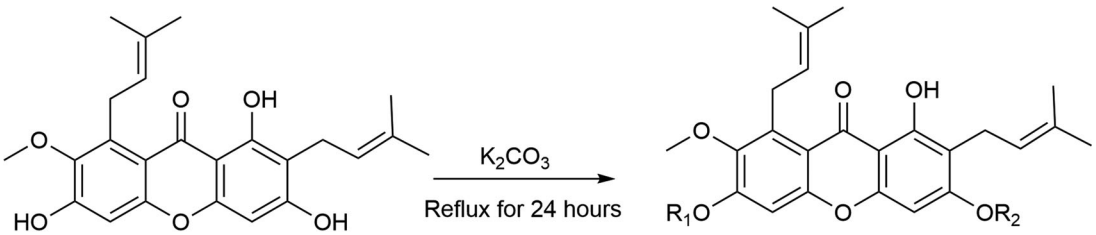

A1: $R_1 = R_2 = CH_3$
A2: $R_1 = R_2 = C_2H_5$
A3: $R_1 = R_2 = C_3H_7$
A4: $R_1 = R_2 = C_4H_9$

SCHEME 1 General reaction scheme of the synthesis of α-mangostin derivatives

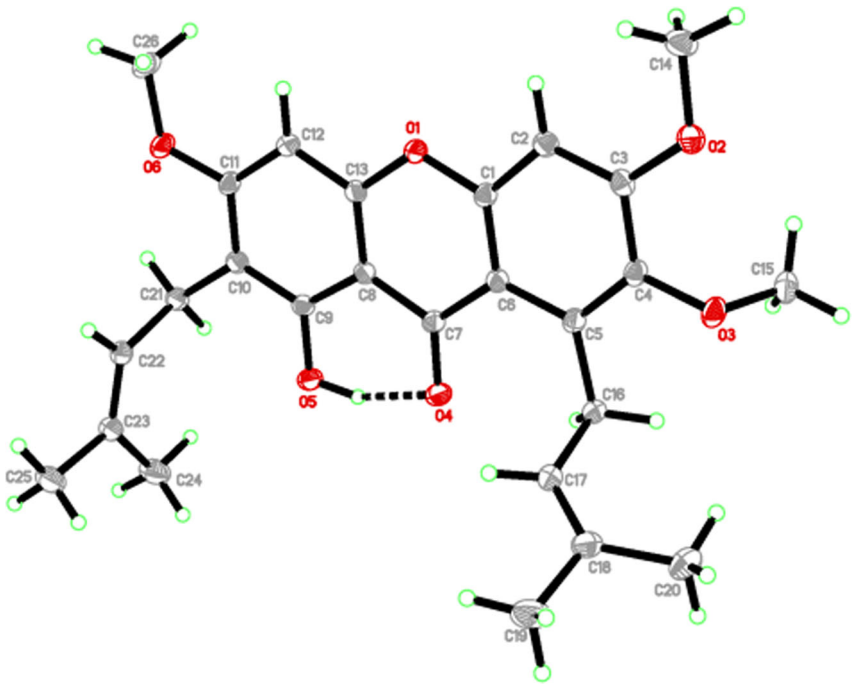

FIGURE 1 The molecular structure of **A1** showing 50% probability displacement ellipsoids for non-H atoms and the atom-numbering scheme. An intramolecular hydrogen bond is shown as a dashed line

and its least-square plane makes dihedral angles of 63.20(6)° and 79.60(6)° with the two planar 2-methylbut-2-ene (root mean square deviations = 0.023 and 0.006 Å) moieties, respectively. The two benzene rings make a dihedral angle of 4.73(6)°. The crystal structure is stabilized by an intramolecular O–H···O hydrogen bond, which forms an *S*(6) ring motif (Figure 1). The crystal structure was found to exhibit no intermolecular hydrogen bonding but instead possesses a weak C–H···π and a π–π stacking interactions between the benzene and 4H-pyran rings (centroid to centroid distance = 3.5794(7) Å).

2.2 | Cholinesterase inhibitory activities

The cholinesterase inhibitory activities of α-mangostin and its derivatives were determined by the Ellman method and the results are summarized in Table 1. In general, the derivatives **A1**–**A4** had comparable AChE selective inhibitory activities with IC_{50} values ranging from 4.15 to 6.73 μM that are 1.7- to 2.7-fold less potent compared with α-mangostin. The AChE inhibitory activities of **A1**–**A4** were improved from methyl to butyl substitutions and **A4** was the most potent inhibitor among the four. However, the inhibitory activities of **A1**–**A4** against BChE were greatly reduced with the IC_{50} values ranging from 26.99 to 129.13 μM, that is, 4.6- to 22.0-fold less potent compared with α-mangostin. It is interesting to note that the AChE selectivity of derivatives was increased up to 21.7-fold by one-step alkylation, the selectivity reduced consistently with an increase in the aliphatic side chain length. For example, the AChE selectivity for derivative **A4** is 6.5 (Table 1), derived from the formula where the IC_{50} against BChE is the nominator and IC_{50} against AChE is the denominator. As the aliphatic side chain length increases from **A1** to **A4**, the IC_{50} values against BChE are greatly reduced, hence their selectivity also reduces.

2.3 | Molecular docking

In silico molecular docking was performed to investigate the interactions between the derivatives **A1**–**A4** and residues at the active site of the enzymes (Figure 2). AChE has an active site that is not on the protein's surface but located at the bottom of a 20-Å-deep gorge, lined largely by aromatic residues.[30] The results showed that **A1**–**A4** could accommodate inside the gorge of AChE. **A1** formed π–π

TABLE 1 Cholinesterase inhibitory activities of the dialkylated derivatives of α-mangostin

Compound	AChE inhibition, IC_{50} (μM)	BChE inhibition, IC_{50} (μM)	AChE selectivity[a]
A1	6.73 ± 0.07	129.13 ± 0.07	19.2
A2	5.04 ± 0.14	109.48 ± 0.99	21.7
A3	4.89 ± 0.10	86.93 ± 1.57	17.8
A4	4.15 ± 0.18	26.99 ± 0.65	6.5
α-Mangostin	2.48 ± 0.11	5.87 ± 0.09	2.4
Galantamine	0.27 ± 0.07	5.55 ± 0.24	20.4

Note: Data are presented as mean ± *SD* (*n* = 3).
Abbreviations: AChE, acetylcholinesterase; BChE, butyrylcholinesterase; *SD*, standard deviation.
[a]Selectivity against AChE: IC_{50}BChE/IC_{50}AChE.

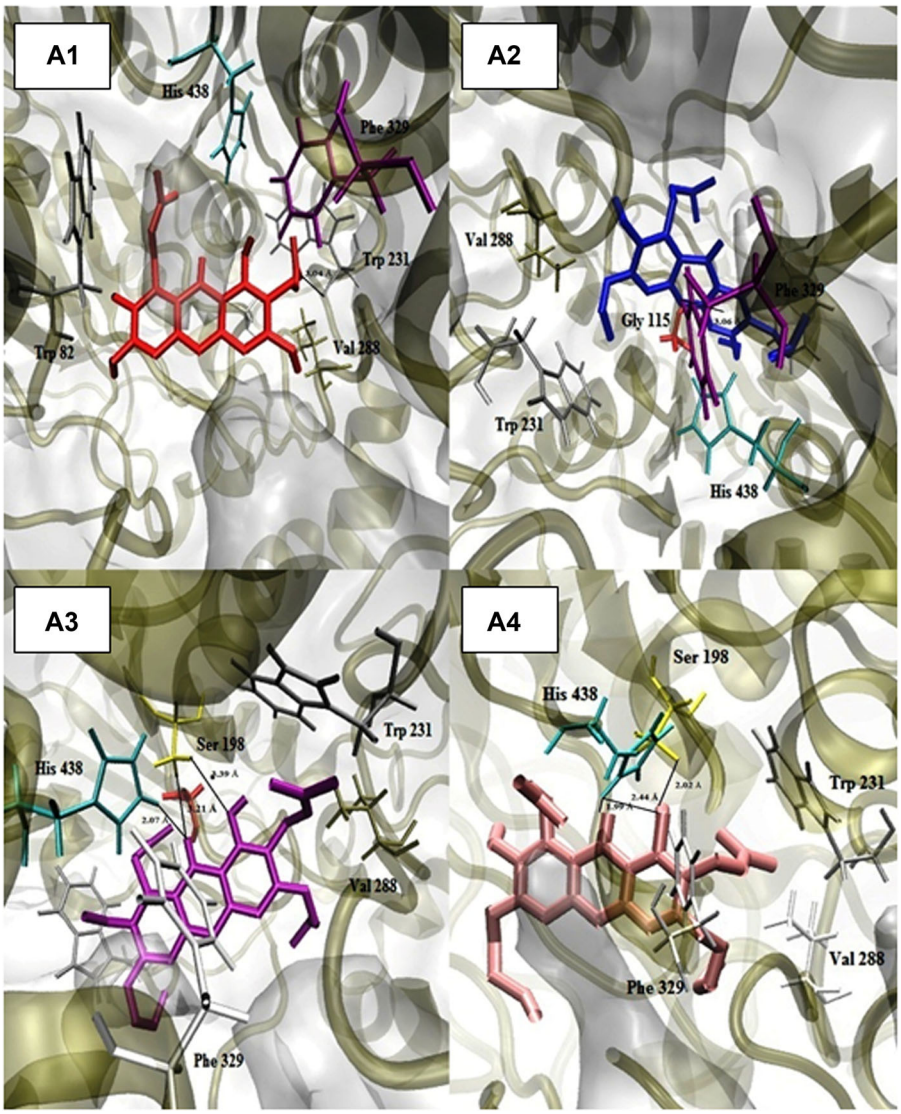

FIGURE 2 Dialkylated derivatives of α-mangostin docked into the binding site of acetylcholinesterase

interaction with Phe330 at the choline-binding site. In contrast, **A4** was unable to penetrate deep into the gorge, probably attributed to the bulkiness of the compound and narrow active site gorge of AChE. The molecular docking result showed that **A4** accommodated close to the choline-binding site, forming σ–π interaction with Phe330 (3.29 Å), which anchored this compound to the *Tc*AChE active site gorge (Table 2). Compound **A4** accommodates in the same orientation as α-mangostin at the middle of the AChE gorge but with

TABLE 2 Binding interactions data for **A1** and **A4** docked into active site gorge of *Tc*AChE

Ligand	Binding energy (kcal)	Enzyme interacting site	Residue	Type of interaction	Distance (Å)	Ligand-interacting moiety (ring)
A1	−11.28	Choline-binding site	Phe330	Hydrophobic	4.64	C
A4	−12.47	Choline-binding site	Phe330	Hydrophobic	3.29	C
α-Mangostin[a]	−12.69	Choline-binding site	Trp84	Hydrophobic	4.75	B
		Choline-binding site	Trp84	Hydrophobic	3.51	A
		Choline-binding site	Trp84	Hydrophobic	5.47	C
		Peripheral anionic site	Asp72	Hydrophobic	2.84	C
		Oxyanionic hole	Gly117	Hydrogen	2.01	A (OH at C-6)

[a]Data taken from Khaw et al.[26]

lesser interactions due to the hydroxyl groups at C-3 and C-6 positions being alkylated. Furthermore, the interaction of **A1** and **A4** with choline-binding site was found to be different compared with α-mangostin.[26] Choline-binding site is located at the middle narrow neck of the gorge, lined by Phe330 and Tyr121 at the upper site and Trp84 at the further down site of the gorge, approximately 15 Å deep.[30] Due to the bulkiness of the derivatives, especially **A4**, they could interact with Phe330 but not Trp84, which is seen with α-mangostin, because α-mangostin could penetrate deeper into the gorge. On the other hand, derivatives **A2** and **A3** did not demonstrate any interactions at AChE active site. Despite being able to dock into the active site there was no hydrogen bonding within a distance of 3.5 Å or hydrophobic interaction within a distance of 7.0 Å between the hydroxyl group or phenolic rings of **A2** and **A3** with the protein residues at the active site. The molecular docking showed an inverse relationship between AChE inhibitory activities (IC_{50}) of the derivatives with their free energy of binding as shown in Figure 3, in which **A1**–**A4** demonstrated good free energy of binding.

2.4 | Cytotoxicity

Few studies reported on the cytotoxicity of α-mangostin in various cell lines. Matsumoto et al.[25] stated that α-mangostin was cytotoxic against human leukemia cells with LC_{50} of 10 μM, while it was highly cytotoxic on breast cancer (LC_{50} of 0.92 μg/ml) and epidermoid carcinoma of the mouth (LC_{50} of 2.08 μg/ml) cell lines. In addition, Nakagawa et al.[23] reported decreased viability of DLD-1 cells upon treatment with 20 μM of α-mangostin.[23] α-Mangostin together with its derivatives, **A1**–**A4**, were tested for their toxicity on human neuroblastoma (SH-SY5Y, SK-N-SH) and human liver cancer (HepG2) cells. Table 3 summarizes the LC_{50} values and the selectivity index of the tested compounds on the three types of cells. Similar to the findings from previous studies, α-mangostin was found to be cytotoxic toward SH-SY5Y, SK-N-SH, and HepG2 cells with LC_{50} of 11.20, 12.16, and 12.71 μM, respectively. Interestingly, all four dialkylated derivatives of α-mangostin showed much lower cytotoxicity, being 6.4- to 9.0-fold and 3.8- to 5.5-fold less toxic than their parent compound on neuroblastoma and liver cancer cells, respectively (Table 3). Likewise, the selectivity index of the derivatives was 1.9- to 4.4-fold higher, in particular, **A2** and **A4** showed improved selectivity index compared with α-mangostin, since both derivatives had a larger ratio of LC_{50}(on respective cells)/IC_{50}(AChE), indicating lower lethality. In other words, derivatives **A2** and **A4** have a bigger therapeutic index, thus they may offer a larger range of safe and effective drug dosing to work with compared with α-mangostin. This finding indicates that the hydroxyl group at positions 3 and 6 may, in part, be responsible for the cytotoxicity of α-mangostin against the tested cells. Derivatization of the hydroxyl group at those positions lowered the cytotoxicity of the parent compound. Our findings are consistent with a study by Fei et al.,[29] which showed that the phenol groups at C-3 and C-6 positions are critical for the anticancer activities of α-mangostin and C-4 modification is capable to improve both anticancer activity and drug-like properties. The findings of the present study prompt a renewed interest in the search for the new cholinesterase inhibitors from α-mangostin with a higher safety margin.

2.5 | Theoretical prediction of ADME properties

The ADME properties of α-mangostin and dialkylated derivatives were predicted in silico using the Accelrys Discovery Studio and the data are summarized in Table 4. Compounds **A1**–**A4** showed comparable ADME properties to α-mangostin with good absorption and plasma protein binding, but lower solubility. In addition, all derivatives followed Lipinski's rule of five (molecular weight, log*P*, number of hydrogen donors, and acceptors) except for **A4** with higher log*P* value and molecular weight over 500. One of the major hurdles for a medicinal chemist is the penetration of potential compounds through the complex blood–brain barrier. Most of the central nervous system active drugs prompt to penetrate into the brain through passive diffusion.[31,32] Interestingly, compound **A1** is predicted to have high

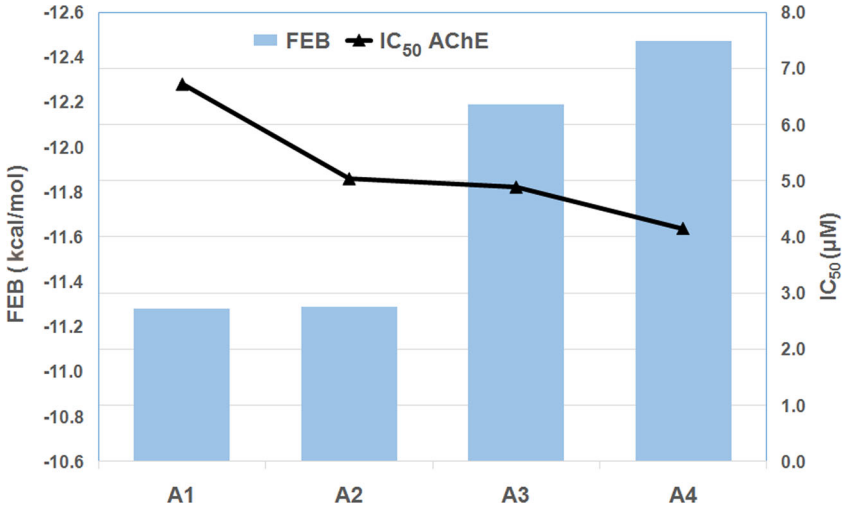

FIGURE 3 Relationship between free energies of binding (FEB) and IC_{50} of isolated compounds. AChE, acetylcholinesterase

TABLE 3 Cytotoxicity of the dialkylated derivatives of α-mangostin

	SH-SY5Y		SK-N-SH		HepG2	
Compound	LC_{50} (μM)	SI[a]	LC_{50} (μM)	SI[a]	LC_{50}	SI[a]
A1	71.92 ± 3.44	10.7	103.99 ± 1.80	15.4	67.79 ± 0.97	10.1
A2	100.94 ± 1.18	20.0	107.85 ± 0.36	21.4	48.46 ± 1.17	9.6
A3	75.98 ± 1.53	15.5	79.36 ± 0.34	16.2	49.52 ± 0.38	10.1
A4	74.00 ± 10.79	17.8	88.18 ± 0.67	21.2	69.38 ± 0.84	16.7
α-Mangostin	11.20 ± 0.09	4.5	12.16 ± 0.16	4.9	12.71 ± 0.26	5.1

Note: Data are presented as mean ± *SD* (*n* = 3).
Abbreviations: AChE, acetylcholinesterase; SI, selectivity index.
[a]SI is defined as LC_{50}(on respective cells)/IC_{50}(AChE).

TABLE 4 Theoretical prediction of ADME properties of α-mangostin and its dialkylated derivatives[a]

Compound	Log*P*	Molecular weight	BBB level[b]	Absorption level[c]	Log*S*[d]	PPB[e]
A1	4.97	439.2	1	0	−5.647	1
A2	5.67	467.2	4	1	−5.992	2
A3	6.71	495.3	4	2	−6.597	2
A4	7.63	523.3	4	3	−7.036	2
α-Mangostin	4.52	410.1	4	1	−4.913	1
Galantamine	1.06	287.3	3	0	−2.668	0

Abbreviations: ADME, absorption, distribution, metabolism, and excretion; BBB, blood–brain barrier; PPB, plasma protein binding.
[a]The data were determined with Accelrys Discovery Studio.
[b]0, 1, 2, 3, and 4 indicate very high, high, medium, low, and undefined penetration, respectively.
[c]0, 1, 2, and 3 indicate good, moderate, low, and very low absorption, respectively.
[d]Log*S* [log(molar solubility)] < −8.0, extremely low; −8.0 < log*S* < −6.0, very low; −6.0 < log*S* < −4.0, low; −4.0 < log*S* < −2.0, good; −2.0 < log*S* < 0.0, optimal; log*S* > 0.0, too soluble.
[e]0, 1, and 2 indicate <90% binding, ≥90% binding, and ≥95% binding with plasma protein, respectively.

blood–brain barrier penetration that is better than the standard drug, galantamine. However, the other derivatives and α-mangostin were predicted to have an undefined blood–brain barrier penetration. For the human intestinal absorption of the compounds, **A1** is predicted to have good absorption similar to galantamine, while **A2** is predicted to have moderate absorption similar to α-mangostin. The derivatives **A3** and **A4** are predicted to have low to very low absorption. Log*S* is the log of molar solubility, which is directly related to the solubility of a compound and defined as the number of moles of the solute that can be dissolved per liter of a solution before saturation. Galantamine is categorized in the good solubility category; α-mangostin, **A1** and **A2** are categorized in the low solubility category whereas **A3** and **A4** are categorized in the very low solubility category. Nevertheless, the low solubility and absorption properties of the derivatives are not a major concern and could be overcome by appropriate formulation to enhance their solubility and absorption. The derivatives **A2**–**A4** are predicted to have >95% protein binding, while **A1** and α-mangostin are predicted to have >90% protein binding. From the pharmacological point of view, compounds having lesser protein binding are considered favorable, especially in a disease state with lower plasma proteins, or in cases of polypharmacy to avoid possible drug–drug interactions via displacement from protein binding.

3 | CONCLUSION

The present study reported on the impact of simple structural modification of α-mangostin on its cholinesterase inhibitory activities and toxicity toward neuroblastoma and liver cancer cells for the first time. All semisynthesized derivatives remained as potent inhibitors of AChE with IC_{50} lower than 10 μM, but moderate to weak BChE inhibition with IC_{50} values up to 130 μM compared with α-mangostin. The nature of protein–ligand interaction with AChE is mainly hydrophobic. In contrast, all the derivatives were less cytotoxic and had a much higher selectivity index than the parent compound. Thus, modification of α-mangostin at position C-3 and C-6 greatly impact its BChE inhibitory activities and cytotoxicity but not AChE inhibitory activities. The dialkylated derivatives are viable candidates for further structural modification and refinement in the search of new AChE inhibitors with higher safety margins.

4 | EXPERIMENTAL

4.1 | Isolation of α-mangostin and semisynthesis of the alkyl derivatives

The fruit pericarp of *G. mangostana* was collected from Penang, Malaysia, and a voucher specimen (No. 11247) of the plant was deposited at the School of Biological Sciences, Universiti Sains Malaysia. α-Mangostin was isolated according to the procedure described previously.[26] The semisynthesis of α-mangostin derivatives was conducted by *O*-alkylation reaction in which the hydroxyl group of the α-mangostin was replaced by the alkyl chain from the alkyl halide (methyl iodide, ethyl iodide, propyl iodide, and 1-chlorobutane). The flow of the reaction is as follows: α-Mangostin was dissolved in acetone and refluxed at about 60–65°C with constant stirring overnight; potassium carbonate was used as a catalyst. The reaction was monitored by developing the product and reactant on thin layer chromatography with the solvent system of hexane and ethyl-acetate (6:4).

The InChI codes of the investigated compounds, together with some biological activity data, are provided as Supporting Information Data.

4.1.1 | Synthesis of A1

The title compound was obtained as pale yellow solid (yield 80.0%) with melting point of 89–95°C. ^{1}H NMR ($CDCl_3$, 500 MHz, δ ppm): 13.47 (1H, s), 6.73 (1H, s), 6.32 (1H, s), 5.23 (1H, m), 4.13 (2H, d, J = 7 Hz), 3.35 (2H, d, J = 7 Hz), 3.79 (3H, s), 3.89 (3H, s), 1.84 (3H, s), 1.79 (3H, s), 1.67 (3H, s), 1.57 (3H, s). ^{13}C NMR ($CDCl_3$, 125 MHz, δ ppm): 182.0, 163.4, 158.0, 155.3, 155.1, 159.8, 144.0, 137.3, 131.7, 131.6, 123.2, 122.3, 104.0, 111.5, 112.1, 98.2, 88.6, 60.9, 55.7, 55.9, 26.1, 25.9, 25.8, 21.3, 18.1, 17.7. Mass 440.2 $[M + H]^+$.

4.1.2 | Synthesis of A2

The title compound was obtained as pale yellow solid (yield 75.0%) with melting point of 100–102°C. ^{1}H NMR ($CDCl_3$, 500 MHz, δ ppm): 13.49 (1H, s), 6.68 (1H, s), 6.26 (1H, s), 5.27 (1H, m), 1.85 (3H, s), 1.80 (3H, s), 3.36 (2H, d, J = 7.4 Hz), 1.68 (3H, s), 3.80 (3H, s), 4.17 (2H, m), 1.48 (3H, t, J = 6.9 Hz), 1.51 (3H, t, J = 6.5 Hz). ^{13}C NMR ($CDCl_3$, 125 MHz, δ ppm): 182.0, 162.7, 159.8, 157.2, 155.2, 155.1, 144.0, 137.1, 131.6, 131.3, 123.3, 122.4, 111.9, 111.4, 103.8, 98.6, 89.2, 64.4, 64.0, 60.7, 26.1, 25.9, 25.8, 21.4, 18.1, 17.8, 14.7, 14.5. Mass 468.2 $[M + H]^+$.

4.1.3 | Synthesis of A3

The title compound **A3** was obtained as yellowish powder (yield 34.1%) with melting point of 87–89°C. ^{1}H NMR ($CDCl_3$, 500 MHz, δ ppm): 13.49 (1H, s), 6.70 (1H, s), 6.28 (1H, s), 5.26 (1H, m), 4.13 (2H, d, J = 5.8 Hz), 4.03 (2H, t, J = 6.6 Hz), 3.98 (2H, t, J = 6.6 Hz), 3.80 (3H, s), 3.37 (2H, d, J = 5.8 Hz), 1.94 (2H, m), 1.85 (3H, s), 1.80 (3H, s), 1. 67 (3H, s), 1.12 (3H, t, J = 5.9 Hz), 1.09, (3H, t, J = 5.9 Hz). ^{13}C NMR ($CDCl_3$, 125 MHz, δ ppm): 182.0, 162.8, 159.8, 157.4, 155.2, 155.1, 144.0, 137.0, 131.6, 131.4, 123.3, 122.5, 111.8, 111.4, 103.8, 98.7, 89.2, 70.3, 69.9, 60.8, 26.1, 25.9, 25.8, 22.5, 22.3, 21.2, 18.1, 17.8, 10.6. Mass 496.3 $[M + H]^+$.

4.1.4 | Synthesis of A4

The title compound **A4** was obtained as yellowish powder (yield 43.2%) with melting point of 88–90°C. ^{1}H NMR ($CDCl_3$, 500 MHz, δ ppm): 6.70 (1H, s), 6.28 (1H, s), 4.13 (2H, d, J = 7.1 Hz), 5.26 (1H, m), 1.80 (3H, s), 1.86 (3H, s), 3.36 (2H, d, J = 7.1 Hz), 1. 67 (3H, s), 3.80 (3H, s), 13.50 (1H, s), 4.03 (2H, t, J = 6.35 Hz), 4.08 (2H, t, J = 6.35 Hz), 1.91 (2H, m), 1.58 (2H, m), 1.02 (3H, t, J = 7.35 Hz). ^{13}C NMR in $CDCl_3$: 182.0, 162.8, 159.8, 157.4, 155.3, 155.1, 144.0, 137.0, 131.6, 131.3, 123.3, 122.5, 111.8, 111.4, 103.8, 98.67, 89.2, 68.5, 68.1, 30.9, 31.1, 26.1, 25.9, 25.8, 21.4, 17.8, 18.1, 19.3, 19.0, 13.8. Mass 524.3 $[M + H]^+$.

4.1.5 | Crystallographic data of A1

Crystal was placed in the cold stream of an Oxford Cryosystems Cobra open-flow nitrogen cryostat[33] operating at 100.0 K. Crystallographic data were collected using a Bruker SMART APEX II CCD diffractometer. SADABS and SAINT software[34] were used for absorption correction and data reduction, respectively. The structure was refined by full-matrix least squares on F^2 and solved by direct methods using the SHELXTL software package. O-bound H atom was in a difference Fourier map and refined freely (O–H = 0.92(2) Å). The remaining hydrogen atoms were positioned geometrically (C–H = 0.95–0.99 Å) and were refined using a riding model, with U_{iso} ~ (H) = 1.2 U_{eq}(C). A rotating-group model was applied for the methyl groups. Crystallographic data for **A1** has been deposited at the Cambridge Crystallographic Data Center (No. CCDC 868385).

4.2 | Biological assays

4.2.1 | Cholinesterase inhibition assay

Cholinesterase inhibitory activities of the synthesized derivatives were evaluated following Ellman's microplate assay. Briefly, for AChE assay, 140 μl of 0.1 M sodium phosphate buffer (pH 8) was first added to each well of a 96-well microplate followed by 20 μl of the test sample (in 10% methanol) and 20 μl of 0.09 unit/ml AChE. After 15 min of pre-incubation at 25°C, 10 μl of 10 mM 5,5′-dithiobis(2-nitrobenzoic acid) was added to each well followed by 10 μl of 14 mM acetylthiocholine iodide. The absorbance of the colored end product was measured at 412 nm at designated intervals for 30 min after the initiation of enzymatic reaction by Tecan Infinite 200 ProMicroplate

spectrometer (Switzerland). For the BChE inhibitory assay, the same procedure was followed except that the enzyme and substrate used were BChE from the equine serum and *S*-butyrylthiocholine chloride, respectively. Galantamine was used as a reference standard. Each sample test was conducted in triplicates. The absorbance of the test sample was corrected by subtracting the absorbance of its respective blank. A set of five concentrations was used to estimate the 50% inhibitory concentration (IC_{50}) of the compounds.

4.2.2 | Cytotoxicity assay

SH-SY5Y, SK-N-SH, and HepG2 cells were seeded at 10,000 cells/well in a 96-well plate, in Dulbecco's modified Eagle's medium supplemented with 50% Ham's F-12 nutrient mixture, 10% fetal bovine serum, penicillin (100 U/ml), and streptomycin (100 μg/ml), and were grown at 37°C in a humidified chamber containing 95% air and 5% CO_2. The cells were allowed to grow for 24 hr. The cell viability was determined using MTT [3-(4,5-dimethylthiazol-2-yl)-2,5-diphenyl tetrazolium bromide] colorimetric assay method. The cells were incubated with different concentrations of compounds ranging from 0.39 to 200 μg/ml for 48 hr. Thereafter, 10 μl of MTT solution (1 mg/ml) was added to the wells and the plate was further incubated for 4 hr at 37°C. The medium was then removed and 100 μl of isopropanol was added to each well and vigorously mixed to dissolve the formazan crystals. The absorbance was measured at 570 nm.

4.3 | Molecular docking

Molecular docking was performed by AutoDock 3.0.5 along with AutoDockTools (ADT) using the Lamarckian genetic algorithm.[35] Energy minimization of the compounds was performed using the Tripos force field with a distance gradient algorithm and a convergence criterion of 0.05 kcal/(mol A) MOE (Chemical Computing Group, Montreal, Canada). The crystal structure of *Tc*AChE in complex with galantamine was obtained from Protein Data Bank (PDB code: 1W6R).[36] *Tc*AChE protein was edited using ADT to remove all water molecules and hydrogen atoms were added. Nonpolar hydrogen and lone pairs were then merged and each atom within the macromolecule was assigned a Gasteiger partial charge. A grid box of 41 × 53 × 41 points, with a spacing of 0.375 Å was positioned at the active site gorge. One hundred independent dockings were carried out per docking experiment.

ACKNOWLEDGMENTS

The authors would like to thank Universiti Sains Malaysia, Malaysia, for providing financial support and research facilities. This project was funded by the Research University Grant (RUI) from Ministry of Higher Education Malaysia and Universiti Sains Malaysia (Grant No. 1001/PFARMASI/815093).

CONFLICTS OF INTERESTS

The authors declare that there are no conflicts of interests.

ORCID

Kooi-Yeong Khaw http://orcid.org/0000-0003-2360-6235

REFERENCES

[1] L. Gales, A. M. Damas, *Curr. Med. Chem.* **2005**, *12*, 2499.
[2] K. S. Masters, S. Brase, *Chem. Rev.* **2012**, *112*, 3717.
[3] M. M. Pinto, M. E. Sousa, M. S. Nascimento, *Curr. Med. Chem.* **2005**, *12*, 2517.
[4] M. E. Sousa, M. M. Pinto, *Curr. Med. Chem.* **2005**, *12*, 2447.
[5] L. M. Vieira, A. Kijjoa, *Curr. Med. Chem.* **2005**, *12*, 2413.
[6] B. Lesch, S. Bräse, *Angew. Chem., Int. Ed.* **2004**, *43*, 115.
[7] D.-J. Jiang, Z. Dai, Y.-J. Li, *Cardiovasc. Drug Rev.* **2004**, *22*, 91.
[8] V. Peres, T. J. Nagem, *Phytochemistry* **1997**, *44*, 191.
[9] J. S. Negi, V. K. Bisht, P. Singh, M. S. M. Rawat, G. P. Joshi, *J. Appl. Chem.* **2013**, *2013*, *9*.
[10] M. Y. Ibrahim, N. M. Hashim, A. A. Mariod, S. Mohan, M. A. Abdulla, S. I. Abdelwahab, I. A. Arbab, *Arab. J. Chem.* **2016**, *9*, 317.
[11] L. G. Chen, L. L. Yang, C. C. Wang, *Food Chem. Toxicol.* **2008**, *46*, 688.
[12] S. Tewtrakul, C. Wattanapiromsakul, W. Mahabusarakam, *J. Ethnopharmacol.* **2009**, *121*, 379.
[13] H. A. Jung, B. N. Su, W. J. Keller, R. G. Mehta, A. D. Kinghorn, *J. Agric. Food Chem.* **2006**, *54*, 2077.
[14] B. Márquez-Valadez, R. Lugo-Huitrón, V. Valdivia-Cerda, L. R. Miranda-Ramírez, V. Pérez-De La Cruz, O. González-Cuahutencos, I. Rivero-Cruz, R. Mata, A. Santamaría, J. Pedraza-Chaverrí, *Nutr. Neurosci.* **2009**, *12*, 35.
[15] G. B. Nelli, A. S. K, E. K. Kilari, *Syst. Biol. Reprod. Med.* **2013**, *59*, 319.
[16] H. W. Ryu, M. J. Curtis-Long, S. Jung, Y. M. Jin, J. K. Cho, Y. B. Ryu, W. S. Lee, K. H. Park, *Bioorg. Med. Chem.* **2010**, *18*, 6258.
[17] J. Pedraza-Chaverri, N. Cardenas-Rodriguez, M. Orozco-Ibarra, J. M. Perez-Rojas, *Food Chem. Toxicol.* **2008**, *46*, 3227.
[18] L. M. Reyes-Fermin, S. Gonzalez-Reyes, N. G. Tarco-Alvarez, M. Hernandez-Nava, M. Orozco-Ibarra, J. Pedraza-Chaverri, *Nutr. Neurosci.* **2012**, *15*, 34.
[19] Y. Wang, Z. Xia, J. R. Xu, Y. X. Wang, L. N. Hou, Y. Qiu, H. Z. Chen, *Neuropharmacology* **2012**, *62*, 871.
[20] A. Kijjoa, M. J. Gonzalez, M. M. Pinto, M. S. Nascimento, N. Campos, I. O. Mondranondra, A. M. S. Silva, G. Eaton, W. Herz, *Planta Med.* **2008**, *74*, 864.
[21] S. Laphookhieo, J. K. Syers, R. Kiattansakul, K. Chantrapromma, *Chem. Pharm. Bull.* **2006**, *54*, 745.
[22] A. R. Han, J. A. Kim, D. D. Lantvit, L. B. Kardono, S. Riswan, H. Chai, E. J. C. D. Blanco, N. R. Farnsworth, S. M. Swanson, A. D. Kinghorn, *J. Nat. Prod.* **2009**, *72*, 2028.
[23] Y. Nakagawa, M. Iinuma, T. Naoe, Y. Nozawa, Y. Akao, *Bioorg. Med. Chem.* **2007**, *15*, 5620.
[24] J. J. Wang, Q. H. Shi, W. Zhang, B. J. Sanderson, *Food Chem. Toxicol.* **2012**, *50*, 3004.
[25] K. Matsumoto, Y. Akao, H. Yi, K. Ohguchi, T. Ito, T. Tanaka, E. Kobayashi, M. Linuma, Y. Nozawa, *Bioorg. Med. Chem.* **2004**, *12*, 5799.
[26] K. Y. Khaw, S. B. Choi, S. C. Tan, H. A. Wahab, K. L. Chan, V. Murugaiyah, *Phytomedicine* **2014**, *21*, 1303.
[27] Z. Guo, *Acta Pharm. Sin. B* **2017**, *7*, 119.
[28] M. Biagiotti, V. M. Pappalardo, M. Rabuffetti, G. Speranza, *Nat. Prod. Res.* **2015**, *29*, 750.
[29] X. Fei, M. Jo, B. Lee, S.-B. Han, K. Lee, J.-K. Jung, S. Y. Seo, Y.-S. Kwak, *Bioorg. Med. Chem. Lett.* **2014**, *24*, 2062.
[30] H. Dvir, I. Silman, M. Harel, T. L. Rosenberry, J. L. Sussman, *Chem.-Biol. Interact.* **2010**, *187*, 10.
[31] Z. Rankovic, *J. Med. Chem.* **2015**, *58*, 2584.

[32] Z. Rankovic, *Blood-Brain Barrier in Drug Discovery: Optimizing Brain Exposure of CNS Drugs and Minimizing Brain Side Effects for Peripheral Drugs*, John Wiley & Sons, Hoboken, NJ **2015**, p. 3871.
[33] J. Cosier, A. M. Glazer, *J. Appl. Cryst.* **1986**, *19*, 105.
[34] G. Sheldrick, *Acta Crystallogr. Sect. C* **2015**, *71*, 3.
[35] G. M. Morris, D. S. Goodsell, R. S. Halliday, R. Huey, W. E. Hart, R. K. Belew, A. J. Olson, *J. Comput. Chem.* **1998**, *19*, 1639.
[36] H. M. Greenblatt, C. Guillou, D. Guenard, A. Argaman, S. Botti, B. Badet, C. Thal, I. Silman, J. L. Sussman, *J. Am. Chem. Soc.* **2004**, *126*, 15405.

How to cite this article: Khaw K-Y, Kumar P, Yusof SR, Ramanathan S, Murugaiyah V. Probing simple structural modification of α-mangostin on its cholinesterase inhibition and cytotoxicity. *Arch Pharm.* 2020;e2000156.
https://doi.org/10.1002/ardp.202000156